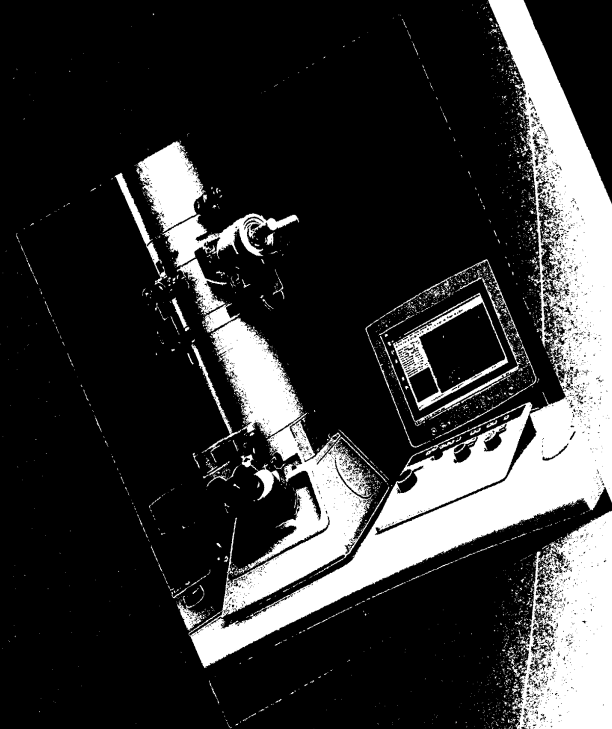


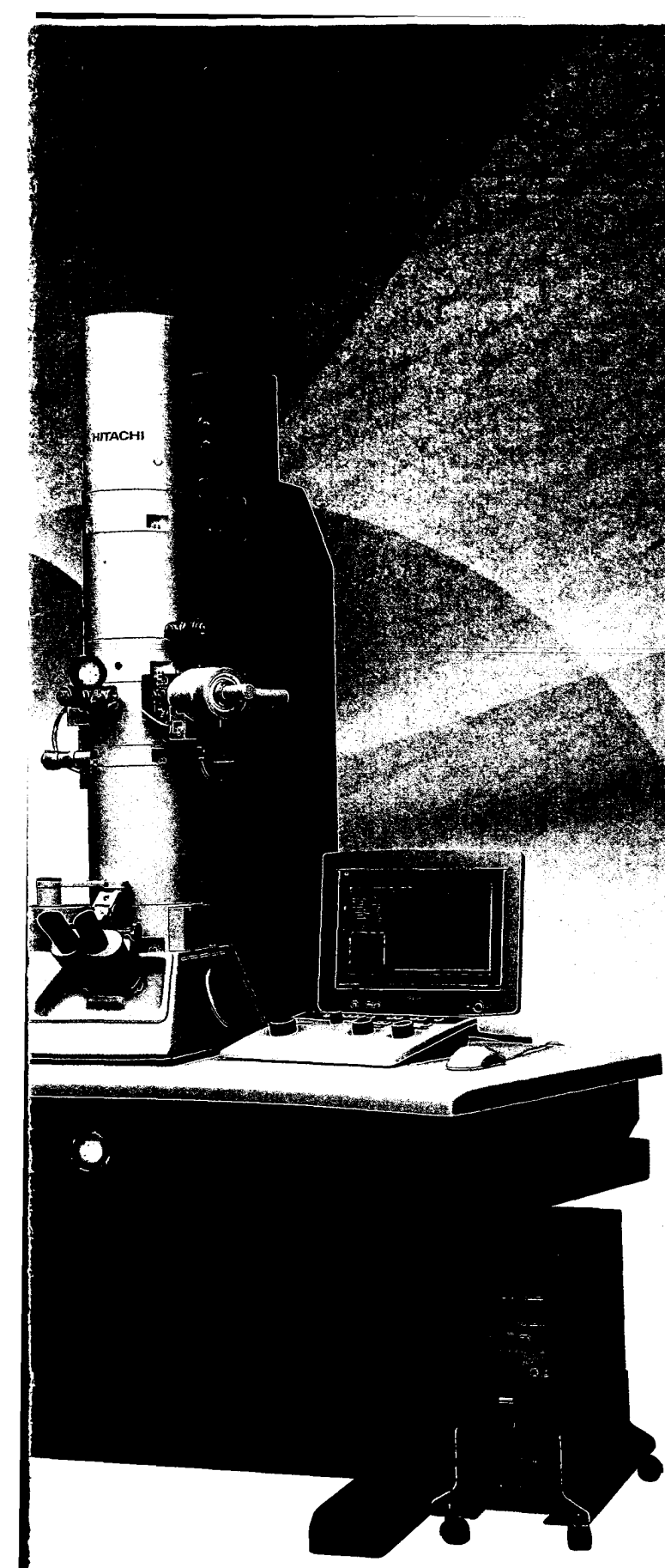
HITACHI

日立電子顕微鏡
H-7600



便りに於ける高機能。

H-7600は透過電子顕微鏡としての汎用性と
分解能、高さの小さな試験条件をもつ、高機能で
快速な操作性を追求したもの。最新の干渉干渉
技術を搭載したPC対応TEM H-7600は画像
撮影機能と干渉干渉方式による強度分析機能、
又機能、又干渉干渉方式による強度分析機能、
ECO方式。



○誰でも撮れる鮮明画像

- ・オートフォーカス／オートステイグマ
- ・アライメントフリー
- ・オートフォトによるフィルム撮影

○操作画面とデジタル画像の同時表示

- ・TVシステム標準装備
- ・Windowsによる制御画面

○容易な視野探し

- ・オートドライブ機能による保存画像の再現
- ・パーソナルデータの管理
- ・撮影条件のデータベース管理

○どこでも使えるIT-TEM

- ・LANやインターネットを利用したリモートオペレーションシステム
- ・データベースによる画像データ管理システム

○低倍率・広視野・高コントラスト像観察

- ・観察倍率700倍、視野径160mm、
対物絞り径10ミクロンで視野カット無し

○高解像度観察

- ・最高倍率60万倍までの高性能ズームレンズ

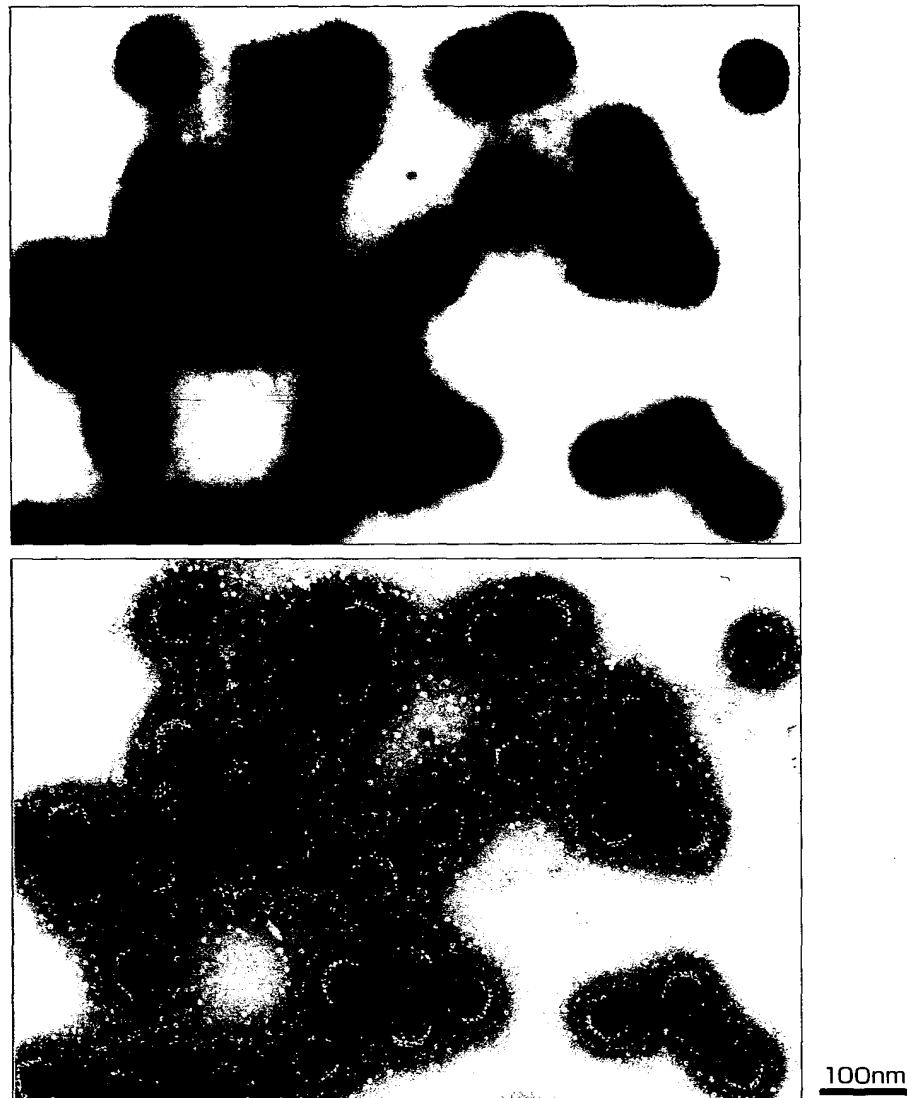
○快適な操作空間

- ・可動式コントロールパネル
- ・広々とした下肢空間
- ・省スペースを追求したコンパクト設計
【設置床面積 25%減(当社従来比)】

○豊富な機能

- ・ロードース機能
- ・測長機能
- ・イメージナビゲーション
- ・オートモニタージュ機能(オプション)
- ・自動粒子検索機能(オプション)
- ・予備照射機能

この上ないシンプル操作で、
際立つ鮮明画像。



〈ネガティブ染色したアデノウイルスを用いたオートフォーカス例〉

試料名:アデノウイルス 総合倍率:120,000倍(撮影倍率 40,000倍) 加速電圧:100kV

(上)オートフォーカスOFF(デフォーカス量:~50μmオーバーフォーカス)

(下)オートフォーカスON(デフォーカス量:~340nmアンダーフォーカス)

(試料ご提供:東京大学分子細胞生物学研究所 豊島 近先生)

アライメントフリー

高圧印加からビーム出しまでワンタッチ操作で完了するので、面倒な軸調整から解放されます。

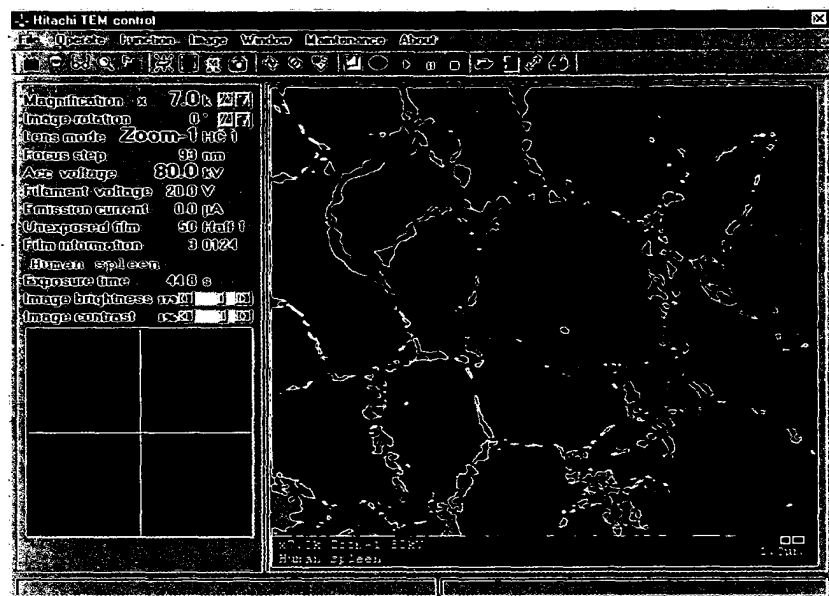
オートフォーカス／オートスティグマ

対物レンズの非点収差補正や焦点合わせを自動化し、高画質のTEM像をすべての人に提供します。
ワンタッチ操作で高精度、高速補正が可能です。

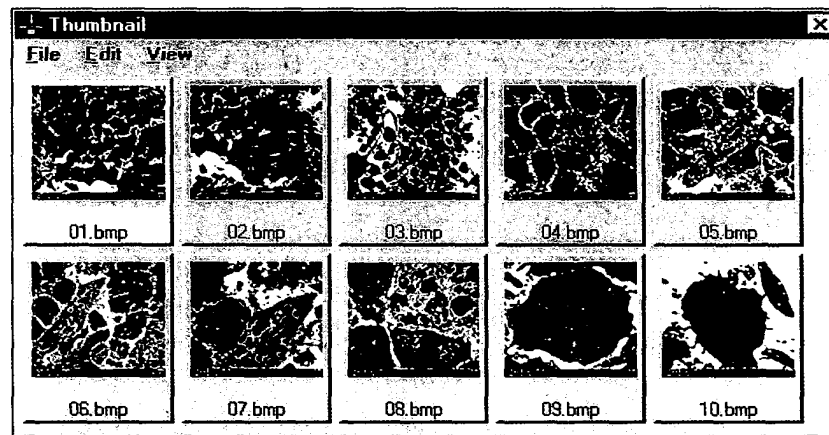
○オートフォト

オートフォーカス・オートスティグマ機能により、フォトボタンを押すだけで最適な写真撮影が完了します。
(オプティマムアンダーフォーカス設定可能)

デジタル画像と画面操作の一体化で、 ワンランク上の利便性を追求。



▼保存画像のサムネイル表示機能



Windows®による操作画面で、観察条件や試料位置などを集中的に表示し、さらに各種機能を見易いアイコンで表示します。

TVカメラのデジタル画像を操作画面上で観察できます。

リアルタイムでのデジタル像観察が可能で、モニタ画面上での視野探しも容易です。

デジタル画像のクイックセーブが可能です。

画像の観察条件や試料位置などのプロパティも保存され、画像のデータベース化が容易です。

スロースキャンCCDカメラをはじめ各種カメラに対応可能です。

※Windowsは、米国およびその他の国における米国Microsoft Corp.の登録商標です。

測長機能

デジタル画像の測長やコメントの入力ができ、さらに画像処理機能が標準で搭載されています。これらの画像はファイル名を変更して保存することができます。

見たい視野を素早く呼び出す、優れた保存・検索機能。

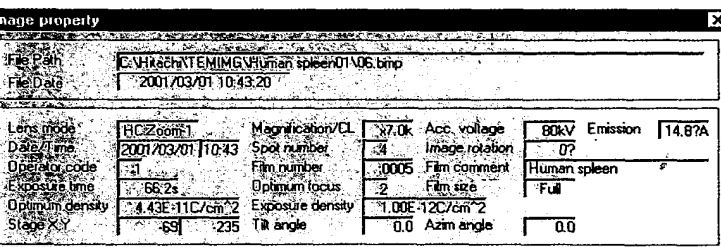
保存画像から試料位置の再現

TVカメラによるデジタル画像はすべてサムネール表示されます。この表示画像をクリックし、オートドライブ機能を選択すると、その画像の観察位置へ自動的に試料ステージが移動します。

Property

Delete

Auto drive



▲Auto-drive機能による試料位置の再現

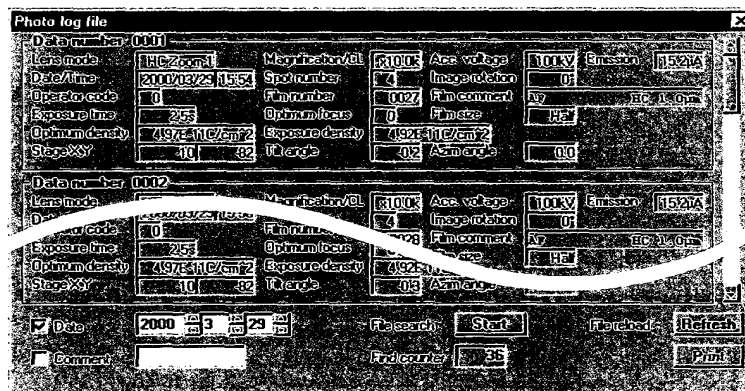
Start

Stop

◀保存画像のPropertyの表示機能

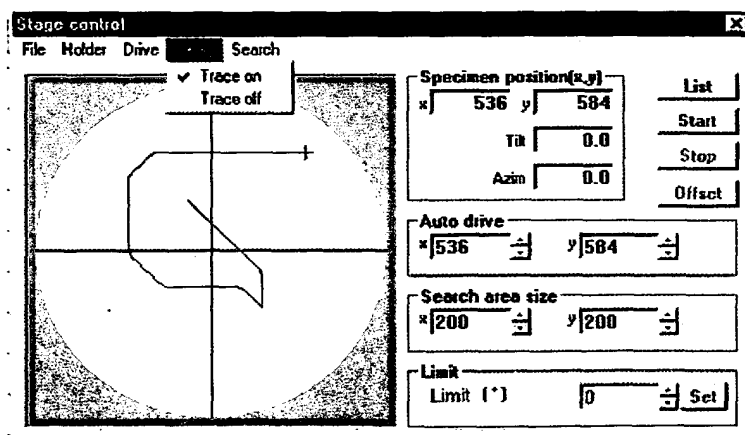
フォトログファイルから撮影試料位置の呼び出し

フィルム撮影の日時やそのときの加速電圧、観察倍率、フィルム印字や露出条件など撮影条件すべてがPCのハードディスクに保存されます。これらの条件から試料座標を呼び出し、その位置を再現することができます。また撮影条件は9999点まで自動記憶され、日付やコメントによる検索も行えます。またExcelでデータ管理も可能です。



イメージナビゲーション

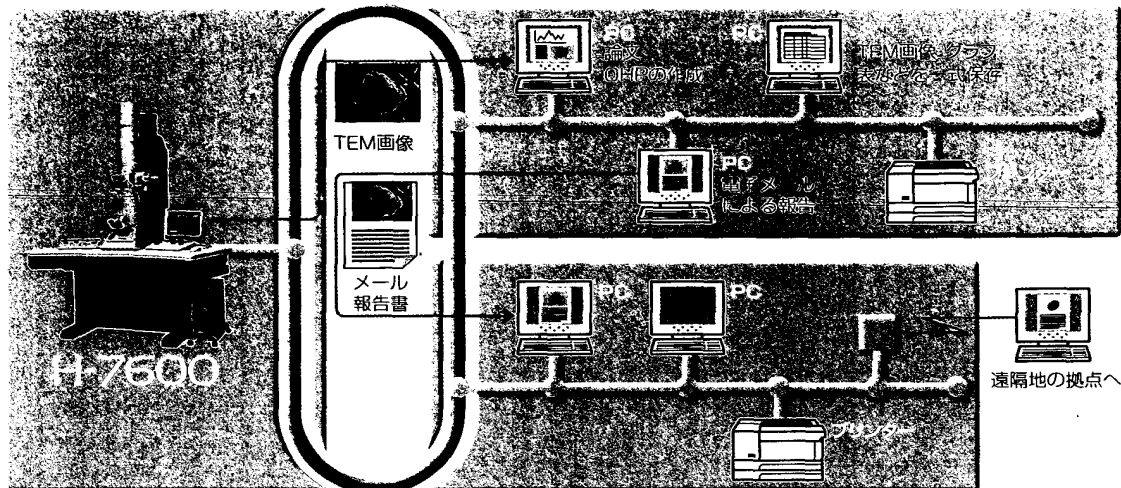
試料位置、傾斜角や方位を最大20点保存することができます。保存した試料位置を呼び出してその位置へステージを移動することも可能です。マイクロトレース機能はステージの移動した軌跡を表示する機能で、観察した領域と未観察領域を容易に確認できます。



さらなる効率化を目指して、進化するIT-TEMの時代。

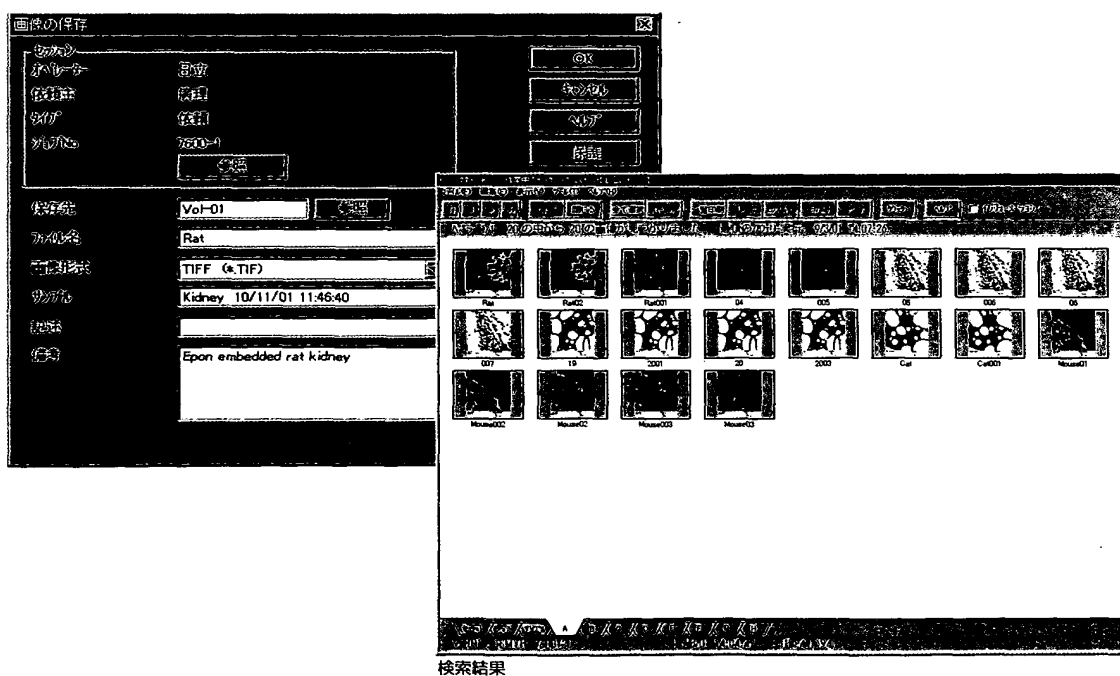
ネットワーク機能（オプション）

TVカメラによるデジタル画像を利用してTEM像のデータベース化が容易です。画像のファイリングはもとより画像の転送によってデータの共有化が図られ、効率的なデータベースの利用が期待できます。さらにLANやインターネットを利用したリモートオペレーション、リモートサービスも可能です。



データベース機能 (PCI) (オプション)

このようにTEM像がデジタルデータになると当然検索が行えるデータベース機能が必要になります。これはTEM像のほか、SEM画像やEDXデータなど各種データを統合して管理できるデータベースソフトの表示例です。



日立独自の最新技術が可能にした、 低倍率・広視野・高コントラスト像観察。

最新の電子光学理論に基づいて設計された日立独自の複合対物レンズの採用により、低倍率での高コントラスト像観察が可能です。観察倍率700倍、直径10ミクロンの対物絞りを用いても直径160mmの蛍光板上で視野カット無しで観察可能です。生物試料ばかりでなく、高分子材料などコントラストの付きにくい試料の観察にも適しています。



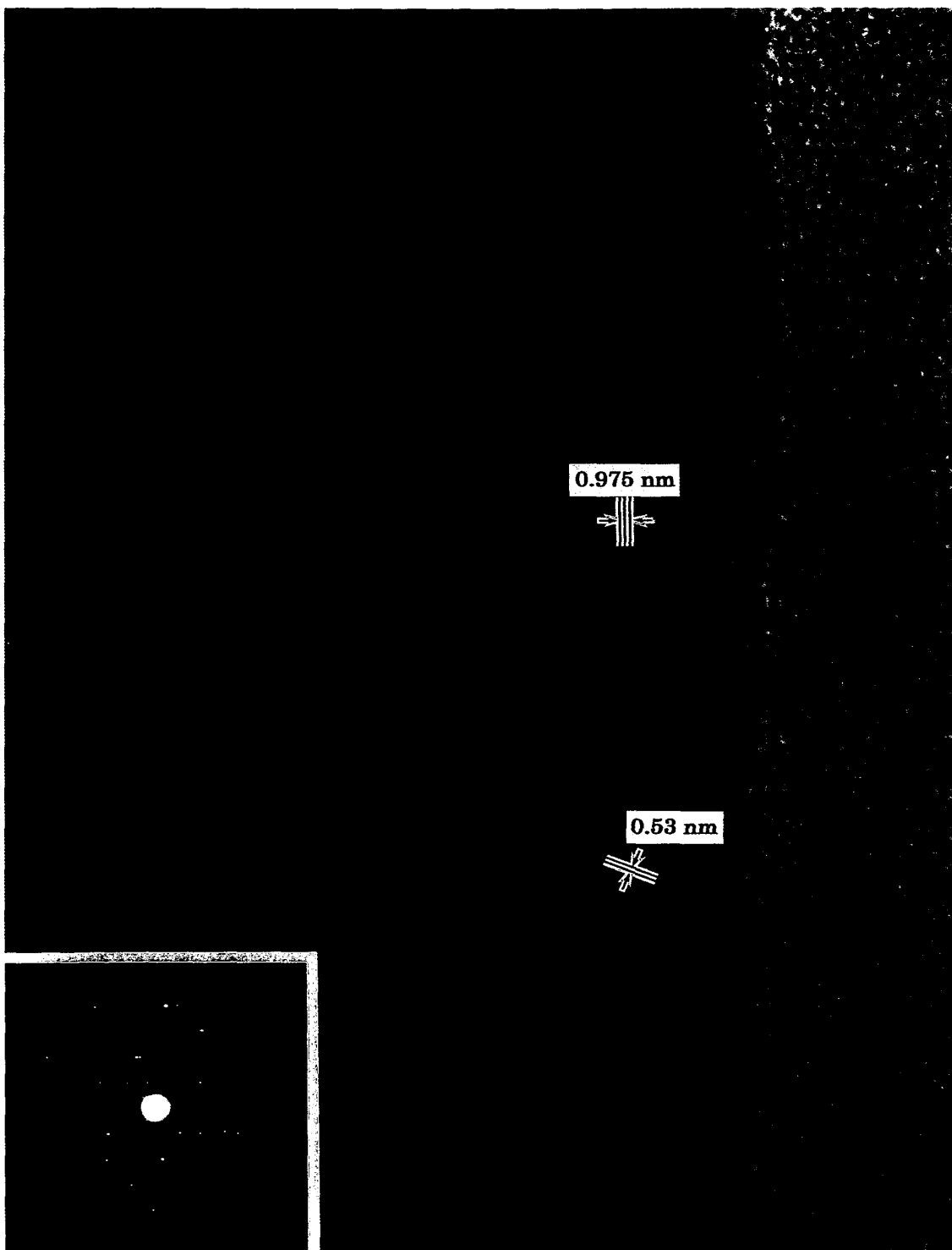
〈HCモードにおける直接倍率700倍の撮影例〉

試料名: マウス腎臓糸球体 総合倍率: 2,300倍 (撮影倍率 700倍) 加速電圧: 80kV

(試料ご提供: 帝京大学医学部附属病院 森本建吾先生)

最高60万倍の高解像度観察も可能。

複合対物レンズの像無回転ズーム機能により、最高60万倍までの安定した高解像度観察が容易です。加速電圧100kVで0.2nm(格子像)の分解能を保証します。下の写真はアスペクトの一種、クロシドライトの高分解能像とその制限視野電子線回折像です。電子線照射に特に弱い試料ですが、纖維の結晶構造が鮮明に観察されています。

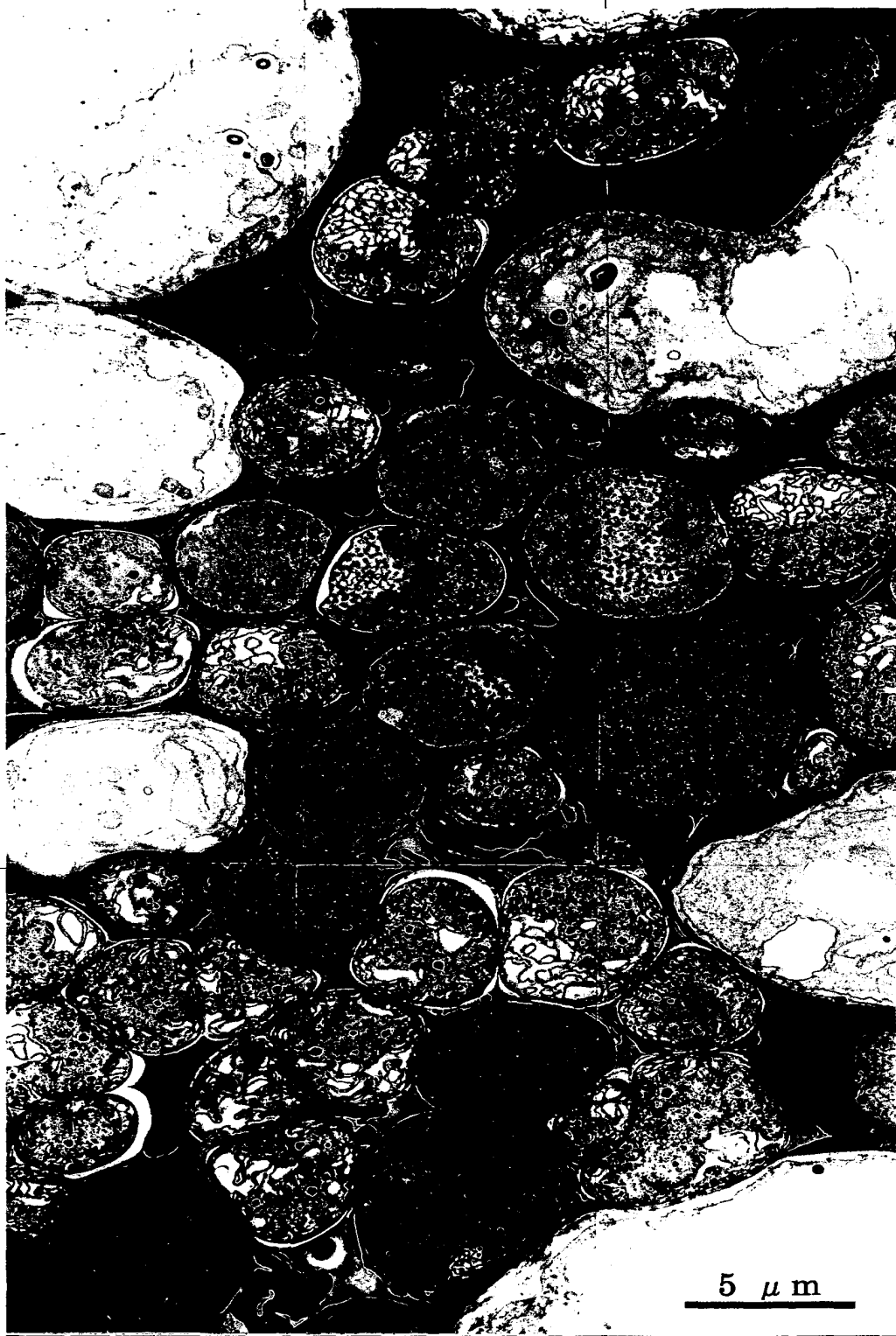


試料名:クロシドライト 総合倍率:1,680,000倍(撮影倍率 200,000倍) 加速電圧:120kV

まさに1枚写真を思わせる驚きの高精度。

オートモンタージュ(オプション)

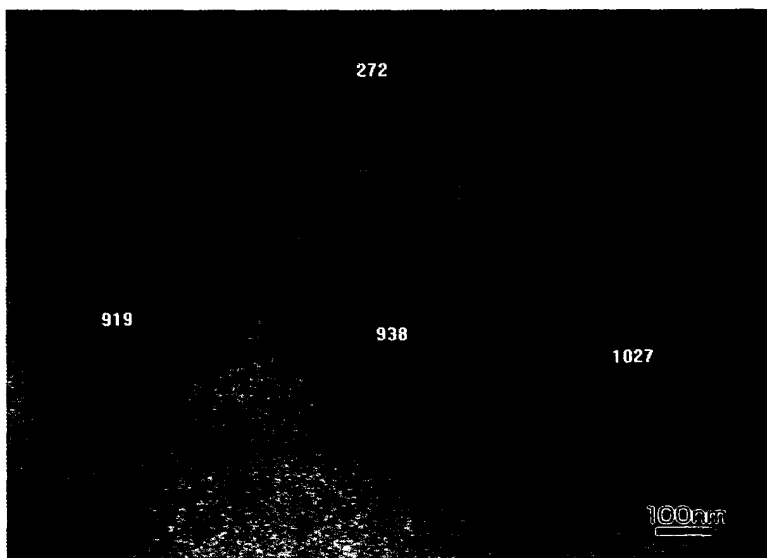
試料ステージの移動から撮影まで、すべてをPC制御し、最大縦横各々11枚、計121枚の連続撮影が可能です。歪みや周辺ボケの小さいレンズにより、高精度のつなぎ写真が得られます。撮影枚数や撮影視野のチェック機能がわかり易くグラフィック表示されています。下の写真はチヂレバツノゴケの9枚連続つなぎ写真(コンタクトプリント)です。歪みもなく、正確につなぎ合わされています。



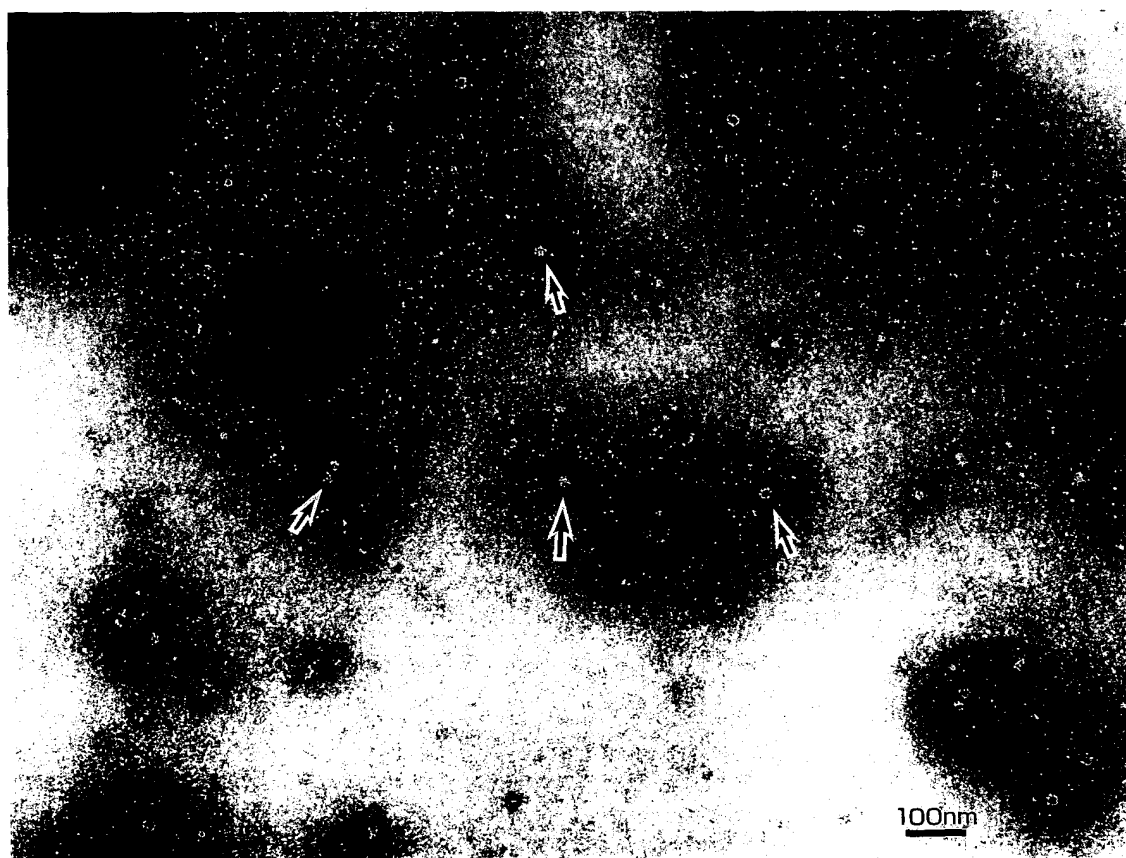
試料名:チヂレバツノゴケ 撮影倍率:5,000倍 加速電圧:100KV
(試料ご提供:埼玉大学理学部 松島 久教授)

ナノサイズの自動粒子検索（オプション）

TEM操作の大半を占める視野探しを自動的に行う機能です。検索粒子の直径、楕円率、検索範囲を設定するだけで、試料ステージが自動的に移動して目的の粒子を検索します。下の写真はヒト小型球形ウイルスの自動粒子検索例です。直径30nm、楕円率1.2の画像パラメータで検索すると、検索されたウイルス粒子がマークされてデジタル画像(a)内に表示され自動保存されます。このデジタル画像のプロパティから検索視野を呼び出して撮影したTEM像(b)には、鮮明にウイルス粒子が観察されています。



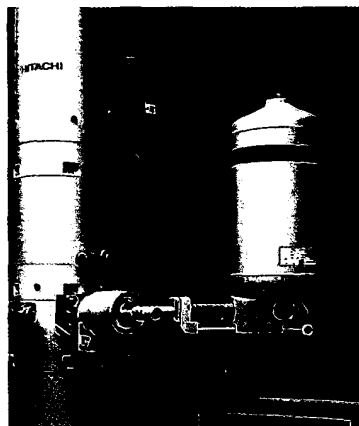
(a)



(b)

試料名:ヒト小型球形ウイルス 総合倍率:75,000倍(撮影倍率 25,000倍) 加速電圧:100kV
(試料ご提供:国立感染症研究所 宇田川悦子先生)

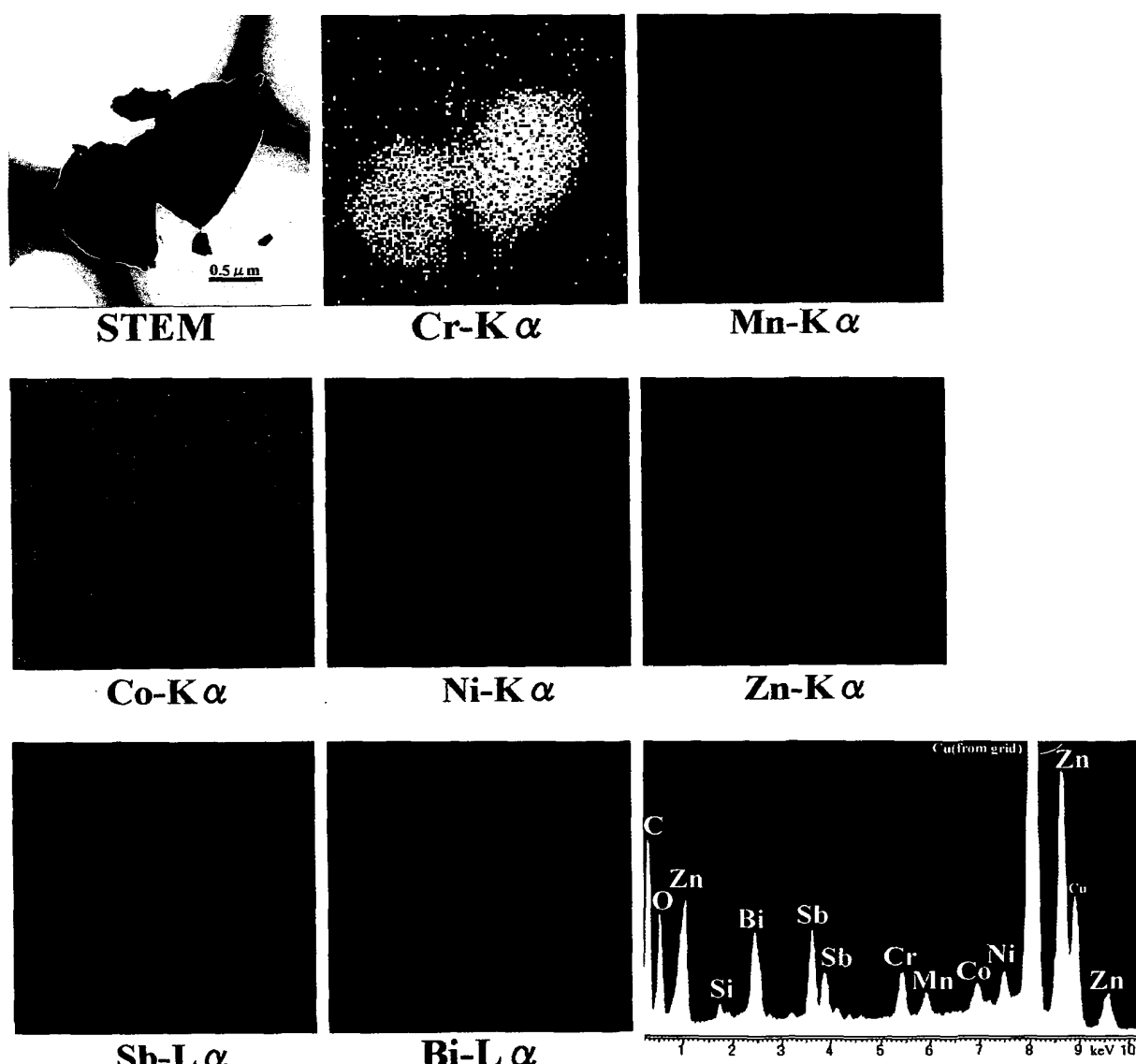
分析機能も充実。



H-7600iにX線分析装置(EDX)を取り付けたところ

X線分析装置(EDXシステム)／ 走査透過像観察(STEM)ユニット(オプション)

サイドティクオフ方式のEDX検出器を採用し、高感度のX線取り込みが可能です。STEMユニットを用いると、多元素同時マッピングやライン分析を行えます。Windows制御のため、操作が容易で、モニタ画面上に表示されたSTEM像はデジタル画像として保存されます。EDX装置とSTEMユニットのモニタおよびキーボードは、ハイマウス(オプション)により共用可能です。

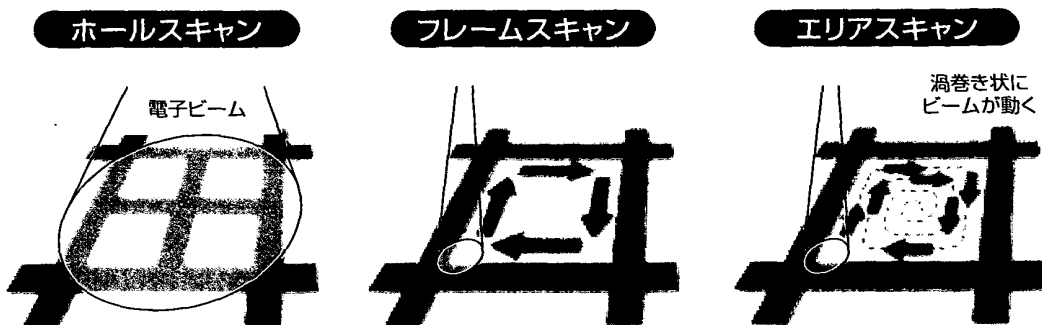


試料名:酸化亜鉛焼結体 観察倍率:30,000倍 加速電圧:100kV

その他にも便利な機能を標準装備。

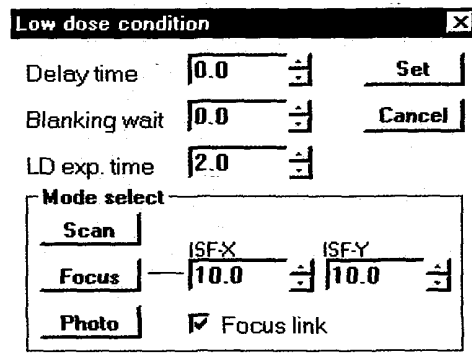
予備照射機能(APIS)

撮影時の試料ドリフトを防止するために、撮影前、あらかじめ予備的に電子線を試料に照射する機能です。各種のモード(ホールスキャン、フレームスキャン、エリヤスキャン)を組み合わせることにより、効果的な予備照射が容易に行えます。



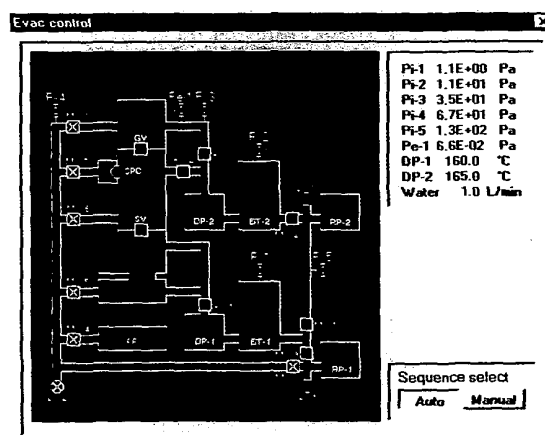
ロードース機能

電子線照射による試料損傷を低減する機能です。撮影領域に電子線を照射することなく焦点合わせを行うため、ネガティブ染色試料や氷包埋試料など電子線照射に弱い試料の観察、撮影に有効です。視野選択のためのスキャンモードやフォーカス、フォトモードなど各種モード、さらに対物レンズ電流値のリンク機能を装備しています。



排気系制御

バルブの開閉や真空度など排気系のシーケンスがわかり易くグラフィック表示されています。完全な差動排気システムにより、試料交換時に加速電圧やフィラメント電圧を切る必要がありません。



豊富な研究用途に対応する 試料ホルダーも、多彩にラインアップ。 (オプション)

H-7600では、研究用途に応じた各種ホルダーを用意しています。

H-7501SS 一軸傾斜ホルダー

H-7502SS ワンタッチ一軸傾斜ホルダー

H-7501MS 三個試料ホルダー

H-7502MS ワンタッチ3個試料ホルダー

H-7501EA X線分析用ホルダー

H-8101DS 二軸傾斜ホルダー

H-7501RS 回転ホルダー

H-7501CS 一軸傾斜冷却ホルダー

H-7501HS 一軸傾斜加熱ホルダー

H-8101UH 一軸傾斜粉体試料加熱ホルダー

H-8101TS 引張りホルダー

上記のほか、Gatan社製クライオトランスマウントホルダーなど各種ホルダーも使用可能です。

H-7501SS 一軸傾斜ホルダー

H-7501MS 三個試料ホルダー

H-7501MS用カートリッジ

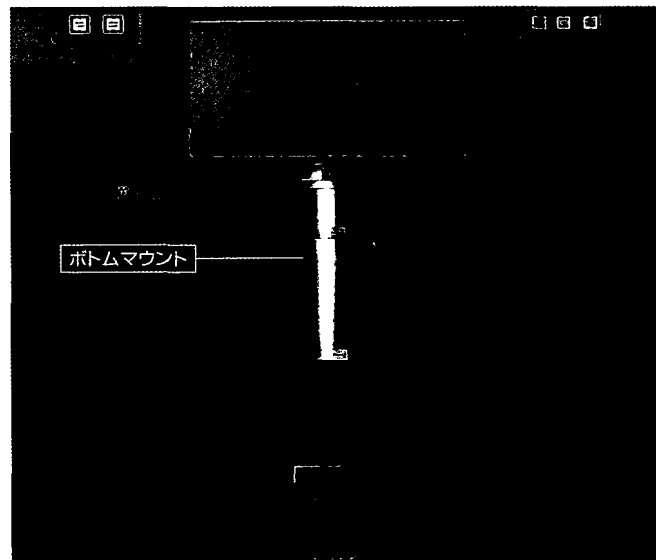
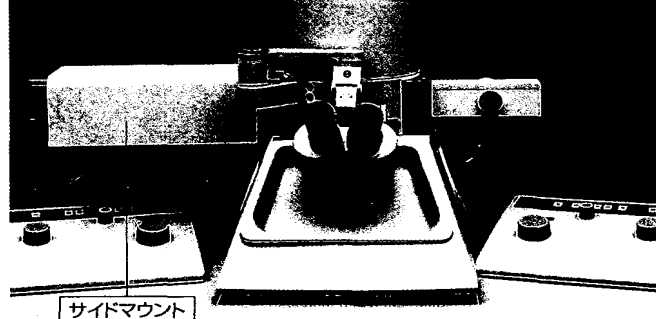
H-7502SS ワンタッチ一軸傾斜ホルダー

H-7502SS 試料抑え部拡大図

H-7501RS 回転ホルダー

デジタルCCDカメラ (オプション)

スロースキャンCCDカメラなどのデジタルカメラを、サイドポートあるいはカメラ室下部に取り付けることができます。



■ 主な仕様

項目	仕様・構成				
分解能	0.2nm(格子像) 0.36nm(粒子像)				
加速電圧	40~120kV				
倍率					
ZOOM	×700~×600,000				
LOW MAG	×50~×1,000				
視野回転機構					
倍率範囲	×1,000~×40,000				
回転角範囲	±90°				
電子線回折カメラ長					
制限視野回折	0.05~8.0m				
カメラシステム	TVシステム	デジタルCCDシステム			
フレームレート	30画/秒	18画/秒			
視野範囲(フィルム上面)	30mm×40mm	110mm×110mm			
画像データ	640×480 ピクセル	1024×1024 ピクセル			
オートフォーカス/オートスティグマ					
使用可能倍率	×700~×100,000				
オートフォト機能付き	自動焦点・露出で撮影可能				
試料汚染低減機能・装置	最適デフォーカス選択可能				
試料換嚢低減機能	鏡体マイロードベーキング機能				
照射レンズ系	ロードース				
レンズ段数	予備照射機能(APIS機能)				
可動絞り					
試料ステージ					
移動範囲	2段				
機能	4段切り替えクリックストップ方式				
結像レンズ系	20, 50, 100, 200μm				
複合対物レンズ	ユーセントリック サイドエントリーゴニオステージ				
対物レンズ可動絞り	試料支持メッシュ3.0mm				
焦点合わせ	X, Y, Z ±1mm	CPU制御によるモータ駆動			
中間レンズ	Z ±0.3mm				
制限視野絞り	イメージナビゲーション機能				
投射レンズ	各観察モード像無回転方式(±5°以内)				
観察室	T型ブロックレンズ				
蛍光板	フォーカスステップ倍率リンク方式				
ビーム検出方式	ニューマ駆動による可動絞りのIN/OUT方式				
撮影機構	(ワンタッチ操作可能)				
フィルム送り	4段切り替えクリックストップ方式				
フィルム装填数	10, 20, 50, 80μm				
フィルムサイズ	ワープラ式焦点合わせ				
視野サイズ	スティグモニタによる焦点・非焦点合わせ				
条件表示	オプティマムフォーカス				
真空排気系	3系統倍率リンク(OF-1, 2, 3)				
真空ポンプ	2段				
真空計	非点補正スティグマトール内蔵				
安全装置	4段切り替えクリックストップ方式				
	50枚(標準) ※100視野撮影可能(50枚装填時)				
	82.5×118mm				
	Full:113×76mm				
	Half:76×53mm				
	CRTによる文字印字				
	倍率、オペレーターコード、フィルムナンバ、加速電圧、				
	コメント(最大20文字)、ミクロンマーカ、年月日 印字可				
	ライナチューブ真空シール方式				
	真空度検知全自動シーケンス制御				
	油抜散ポンプ:570l/s 2式 ※水冷バッフル・バッファタンク付き				
	油回転ポンプ:160[l/s] 2式				
	ピラニ真空計 5式				
	ベニング真空計 1式				
	停電安全装置、断水安全装置、DP温度安全装置、				
	高圧放電安全装置、パワートランジスタ過熱安全装置、				
	各部真空排気安全装置				

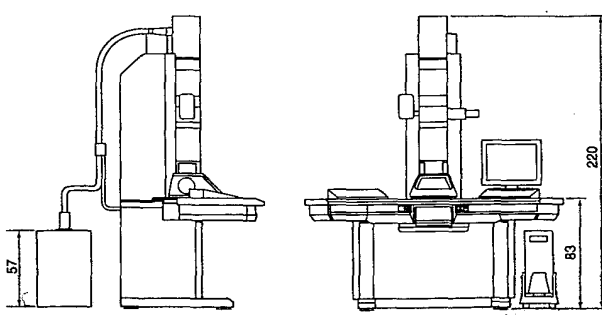
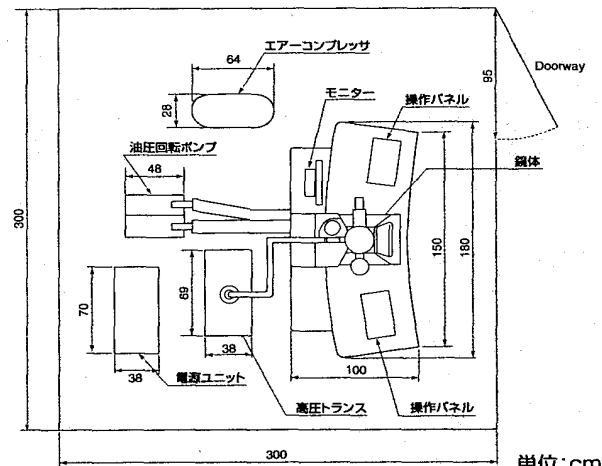
■ 主なオプション

LaB ₆ フィラメント	デジタルCCDカメラ
外部CPUユニット	トラッカーポール
ビームストップバー	コールドフィンガー
オートモントラッシュ	コールドトラップ
自動粒子検索機能	フレートリザーバー
走査透過像観察ユニット	ドライ排気システム
X線分析装置(EDXシステム)	

■ 据付条件

所要電源/必要電力	6.0kVA 単相100V 50Hz/60Hz (STEMユニット付きの場合は6.5kVA)	
電圧変動率	±10%以内 専用設置端子(1000以下) 1個	
給排水		
水温	10~20℃	水温変化±0.1℃/min
水量	2~3l/min×2	系統一 (冷却水循環装置の冷却能力:約3,500W)
水圧	49~196kPa	
給水栓	Rc 3/8(管用テーパめねじ)	2個
排水口	自然排水	2個
外部振動	0.15μT	
	周波数	振幅
	5Hz以下	0.4μmp-p以下
	5Hz~10Hz	1μmp-p以下
	10Hz以上	3μmp-p以下
設置室	温度 15~25℃	
	湿度 60%PH以下	

■ 据付図



安全に関するご注意

○ご使用の前に「取扱説明書」をよくお読みのうえ正しくご使用ください。

○サービスのお問合せは。。。。

日立計測器サービス株式会社

卷 105877 中国科学院植物研究所 1943年4月
植物标本室

卷之三十一

地雷(15.5cm)	1301	88.72400	地雷	英(火炮)	100	460-480
索(地雷)	1302	88.42230	索雷	英(火炮)	340	1500
索(地雷)	1303	88.48000	索雷	英(火炮)	340	1500
破雷	1304	88.12300	破雷	英(火炮)	340	1500
地雷(15.5cm)	1305	88.53500	地雷	英(火炮)	100	460-480
索(地雷)	1306	88.54200	索雷	英(火炮)	340	1500

URL <http://www.hitachi-hitec.com/science/>

URL <http://www.hisco.co.jp>

お問い合わせは――

Penetration and energy-loss theory of electrons in solid targets

K KANAYA† and S OKAYAM

Electrotechnical Laboratory, Mukodai-cho 5-4-1, Tanashi-shi, Tokyo, Japan

MS received 5 April 1971, in final form 4 October 1971

Abstract. Starting from a simple atomic model giving the potential between electrons and atoms as $V(r) = Ze^2a^{s-1}/sr^s$ with the empirical value $s = \frac{3}{2}$, we combine the diffusion effect due to multiple collisions and the energy retardation in accordance with a modified Thomson-Whiddington law, with the scattering cross section in the Lenard absorption law. On this basis, consistent expressions are obtained for the fraction of transmitted electrons in amorphous solid targets, the backscattering fraction with depth, the fraction of electrons absorbed per unit mass-thickness and the depth-dose function, which are in good agreement with experiments over the energy range 10–1000 keV.

A diffusion model represented by a sphere whose centre is located at the maximum energy dissipation depth, related to the diffusion depth and the range, is found to agree well with experiments.

1. Introduction

An explanation of the phenomena connected with electron penetration into solid materials requires information about the attenuation of the electron beam in both numbers and energy. Electron penetration into solid materials has been studied for over 70 years. Most of the relationships have been obtained either by experiments with a high-energy beam (Lenard 1895) or by theoretical considerations under assumptions which are also applicable only at high energies (Bothe 1933, 1949, Bethe 1933, Bethe *et al* 1938). Furthermore, important papers by Wentzel (1922, 1927), Molière (1947, 1948), Lenz (1954), Marton *et al* (1962) and Smith and Burge (1963) were concerned with plural scattering events. The results have been presented in a collected and generalized form by Cosslett and Thomas (1964a,b, 1965), based on the experimental data with the quantitative discussions. Many experimental results have been reported in the field and compared with the different collision models and various theories by Goudsmit and Saunderson (1940), Spencer (1955), Lenz (1958), Meister (1958), Archard (1961), Everhart (1960), Makhov (1960a,b,c), Shimizu and Shinoda (1963) and Dashen (1964).

A simple and semi-empirical theory of electron scattering in solid materials may be required in connection with electron probe microanalysis, scanning electron microscopy, electron beam microrecording and micromachining. When a stream of electrons penetrates into a solid target, electrons may be scattered either elastically or inelastically. Electronic stopping is due to inelastic collisions with atomic electrons in which the incident electron excites or ejects atomic electrons with loss of energy. The corresponding momentum transfer is small because electrons are light particles, but the energy loss is very large. Nuclear stopping, on the other hand, arises from nearly elastic collisions with atomic nuclei, with transfer of both energy and momentum.

† Now at University of Kogakuin, Nishi-shinjuku 1-24-2, Shinjuku-ku, Tokyo, Japan.

Thus electrons are supposed to travel straight into the target, suffering energy loss due to the electronic collisions, and also to be deflected by the nuclear collisions. Back-scattering electrons are those elastically scattered mainly due to nuclear scattering. The plasmon excitation also affects the energy loss of electrons in the solid. Even though the cross section of plasmon excitation is greater, the energy loss seems to be generally small compared with the energy dissipation due to the electronic collision. Therefore the plasmon effects are neglected in this simple theory.

A quasi-elastic scattering theory by Lindhard *et al* (1963) for a stream of ions penetrating into a solid target, which takes into account both types of stopping, may be applied. The cross sections of the nuclear and electronic collisions are derived from an atomic model represented by the power potential $V(r) = Ze^2 a^{s-1} / sr^s$, with $s = \frac{1}{3}$, and the maximum range for the accelerating voltage from 10 to 1000 keV, which is proportional to the incident energy $E_0^{5/3}$, is compared with the most reliable calculation by Berger and Seltzer (1964) and the experimental results Cosslett and Thomas (1964b).

Accordingly, the semi-empirical expressions for the fractions of transmission, back-scattering and absorbed energy are obtained as a function of the reduced depth $y = x/R$, which may be available for different target materials and the wide energy range. Furthermore, after comparing the results obtained by the present theory with the Archard diffusion model, we propose a modified diffusion model. The model, represented by a sphere whose centre is located at the maximum energy dissipation depth, related to the diffusion depth and the range, may give an explanation to the experiments by many authors.

2. Nuclear and electronic scattering cross section

After Lindhard's theory concerning ion-beam scattering, the potential $V(r)$ between the electron and the target atom is assumed to be

$$V(r) = Ze^2 a^{s-1} / sr^s \quad (1)$$

with

$$a = 0.8853 a_H Z^{-1/3}$$

where Z is the atomic number of the target, e the electronic charge and a the effective screened radius of the atom. The number $0.8853 = (9\pi^2)^{1/3} 2^{-7/3}$ is the familiar Thomas-Fermi constant and a_H is the Bohr radius of the hydrogen atom (5.292×10^{-8} cm). s is a numerical parameter: $s=1$ corresponds to Rutherford scattering and $s=2$ to $dE/dx=\text{constant}$. The differential scattering cross section for angular scattering is given by

$$d\sigma_\phi = \frac{\pi a^2}{2 t^{3/2}} f_s(t^{1/2}) dt \quad (2)$$

with

$$f_s(t^{1/2}) = \lambda_s t^{1/2-1/s}$$

where $t = \epsilon^2 \sin^2 \phi/2$; $\epsilon = a/b$ and ϕ is the deflection angle in the centre of gravity system. b is the collision diameter and λ_s is a constant determined empirically. On the other hand, the differential scattering cross section for the energy transfer is derived from (2) and $t = (a/b)^2 T/T_m$:

$$d\sigma_T = \lambda_s \frac{\pi a^2}{2} \left(\frac{b}{a}\right)^{2/s} \frac{T_m^{1/s}}{T^{1+1/s}} dT \quad (3)$$

where T and T_m are the energy transfer and its maximum value.

For the special case of $s = \frac{6}{5}$, which gives good agreement with empirical results in the energy range, the differential nuclear scattering cross section is rewritten from (2) and $b = Ze^2/E$:

$$d\sigma_n = \lambda_s \frac{2^{11/6} \pi a^{1/3} e^{10/3} Z^{5/3}}{4E^{5/3}} \frac{\sin \theta d\theta}{(1 + \cos \theta)^{11/6}} \quad (4)$$

where

$$\theta = \pi - \phi.$$

When we consider the electron penetration in the target, electrons suffering deflections more than 90° do not travel into the subsequent layers of the target and the cross section is given by integration from $\theta = 0^\circ$ to 90° as a first approximation. As was pointed out by Archard (1961), many electrons are deflected between 0° and 90° , and some of them are lost by a multiple collision effect which we will now describe. Consider an electron initially deflected at 45° : it must suffer a second deflection of 45° in the opposite sense to get back into its original direction; but it might equally be deflected by 45° in the same sense, thereby acquiring a total deflection of 90° and becoming lost to subsequent layers. Thus a second approximation for the cross section has been given by adding half the integration from $\theta = 90^\circ$ to 135° . But the correction may be not enough, since the triple and more collisions must exist in fact, as shown in figure 1. The better approximation may be expressed by

$$\int_0^{\pi/2} \frac{\sin \theta d\theta}{(1 + \cos \theta)^{11/6}} + \frac{1}{2} \int_{\pi/2}^{3\pi/4} \frac{\sin \theta d\theta}{(1 + \cos \theta)^{11/6}} + \frac{1}{3} \int_{\pi/2}^{5\pi/6} \frac{\sin \theta d\theta}{(1 + \cos \theta)^{11/6}}$$

and the value of 3.33 is used as an empirical value in the following calculation.

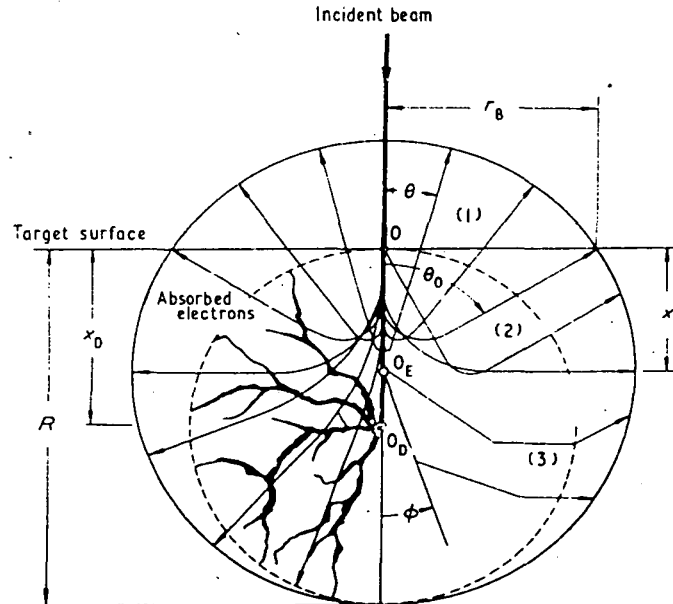


Figure 1. Modified diffusion model of electron-beam penetration in a target: R is the maximum range; x_D the diffusion depth; x_B the maximum energy dissipation depth; r_B the backscattering range; $\tan \theta_0 = r_B/x_B$. (1), (2) and (3) refer to the number of times the electrons are deflected.

Then the total scattering cross section for the angular deflection due to the nuclear collisions is expressed by

$$\sigma_n = \lambda_s \frac{2.97 \pi a^{1/3} e^{10/3} Z^{5/3}}{E^{5/3}} \quad (5)$$

On the other hand, the differential cross section for energy loss due to the electronic collisions is derived from (3) and $b = 2e^2/E$:

$$d\sigma_e = \lambda_s \frac{\pi a^2}{2} \left(\frac{2e^2}{aE} \right)^{5/3} \frac{T_m^{5/6} dT}{T^{11/6}} \quad (6)$$

and resultant energy loss is obtained as follows:

$$\begin{aligned} \frac{dE}{dx} &= NZ \int_0^{T_m} T \frac{d\sigma_e}{dT} dT \\ &= \lambda_s \frac{3 \times 2^{5/3} \pi a^{1/3} e^{10/3} NZ}{E^{2/3}} \end{aligned} \quad (7)$$

where N is the number of atoms per unit volume in the target. The two equations (5) and (7) are the fundamental relationships of elastic (nuclear) and inelastic (electronic) scattering theory.

3. Range-energy relationship

The maximum range can be derived from the energy-loss equation (7):

$$\begin{aligned} R &= \int_0^{E_0} \frac{dE}{dE/dx} \\ &= \frac{E_0^{5/3}}{\lambda_s \times 5 \times 2^{5/3} \pi a^{1/3} e^{10/3} NZ} \end{aligned} \quad (8)$$

where the number N is given by $N = N_a \rho / A$; N_a is the Avogadro number, 6.023×10^{23} ; ρ (g cm⁻³) the density; A (g) the atomic weight; and E_0 (eV) the incident energy. Then the mass-range ρR can be expressed by

$$\rho R = 5.025 \times 10^{-12} A E_0^{5/3} / \lambda_s Z^{8/9} \quad (9)$$

This relationship satisfies qualitatively the experimental results of Makhov (1960a,b,c) and Schumacher (1967) in respect of the dependence of incident energy E_0 and atomic number Z . Good agreement with experiments from 10 to 1000 keV is obtained by taking $\lambda_s = 0.182$. Equation (9) can be rewritten under the relativistic corrections of energy $E_0(1 + 0.978 \times 10^{-6} E_0)/(1 + 1.957 \times 10^{-6} E_0)$ and $a = 0.8853 a_H Z^{-1/3} \times (1 + 1.957 \times 10^{-6} E_0)^{-1}$:

$$\rho R = \frac{2.76 \times 10^{-11} A E_0^{5/3}}{Z^{8/9}} \frac{(1 + 0.978 \times 10^{-6} E_0)^{5/3}}{(1 + 1.957 \times 10^{-6} E_0)^{4/3}} \quad (10)$$

Figure 2 shows a comparison of the voltage dependence of mass-range for several target materials by (10) with the experimental (Cosslett and Thomas 1964b) and calculation results (Berger and Seltzer 1964).

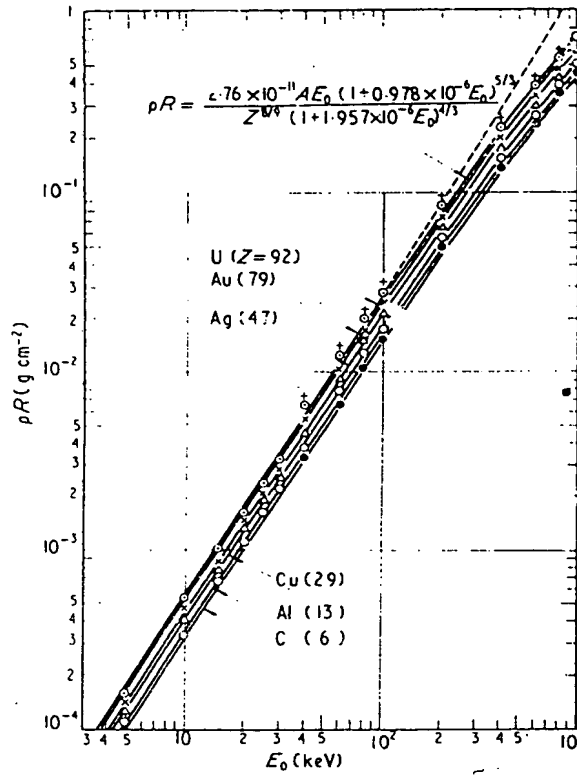


Figure 2. Voltage dependence of mass-range for several targets. Experimental points: + U; o Au; x Ag; triangle Cu; circle Al; bullet C.

From equations (7) and (8) the energy E of electrons at depth x is simply expressed in terms of the reduced depth $y = x/R$:

$$E = (1 - y)^{3/5} E_0. \quad (11)$$

Using the above relation of energy retardation, we can obtain, consistently, the fractions of transmission, backscattering and absorption as functions of y .

4. Transmission and diffusion depth

The general form of variation with thickness in the fraction η_T of the incident current which is transmitted into the forward hemisphere as shown in figure 1 may obey an exponential relation similar to the Lenard law—

$$\eta_T = \frac{i}{i_0} = \exp(-N\sigma_n x). \quad (12)$$

The total scattering cross section σ_n (equation (5)) is connected with the fractional range-energy relationship (11) such that

$$\sigma_n = \lambda_s \frac{2.97 \pi a^{1/3} e^{10/3} Z^{5/3}}{(1 - y) E_0^{5/3}}. \quad (13)$$

By substituting (8) and (13) into (12), η_T can be expressed as a function of γ and y :

$$\eta_T = \exp \left(-\frac{\gamma y}{1-y} \right). \quad (14)$$

The parameter of γ involves the effects of diffusion loss due to multiple collisions for returning electrons and energy retardation due to electronic collisions. It is related to the atomic number alone as follows:

$$\gamma = \frac{2.97}{5 \times 25/3} Z^{2/3} = 0.187 Z^{2/3}. \quad (15)$$

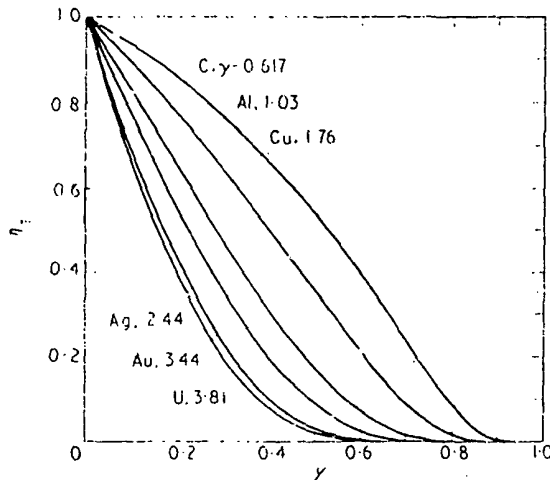


Figure 3. Transmissions of electrons in several targets as a function of the fractional range y . $\eta_T = \exp \{-\gamma y/(1-y)\}$.

Figure 3 shows the variation of η_T in several target materials as a function of y . For an element of low Z (such as carbon), the value of η_T is too small in the region $0 \leq y \leq 0.3$ because of the overestimation of scattering cross section in this region. For elements of high Z (such as copper, silver, gold and uranium), the values calculated by (14) agree closely with the experimental results by Seliger (1955) and Cosslett and Thomas (1964a). Fractional electron transmission η_T for copper as a function of mass-thickness ρx is shown in figure 4.

From the definition of the diffusion depth x_D where the transmitted fraction is $1/e$, it follows that

$$x_D = \frac{R}{1+y} = \frac{R}{1+0.187 Z^{2/3}} \quad (16)$$

which seems to be more reasonable than the expressions given by Meister (1958), Archard (1961) and Tomlin (1963) and accords well with the Monte Carlo calculations by Bishop (1965, 1967). The calculation results from (16) are compared with the experiments by Cosslett (1964) and Seliger (1955) in figure 5.

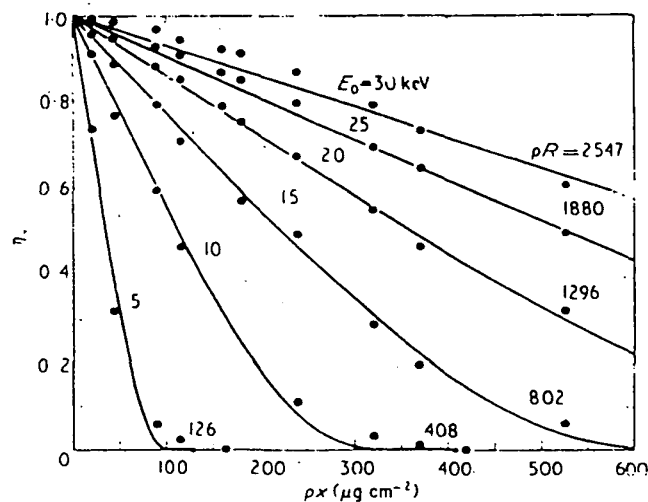


Figure 4. Fractional electron transmission η_T for Cu (29) ($\gamma = 1.76$) as a function of mass-thickness at several values of incident energy E_0 , compared with experimental results (●) of Cosslett and Thomas (1964a).

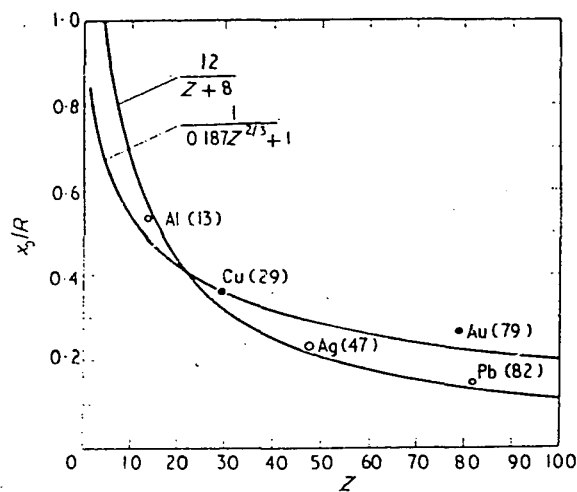


Figure 5. Values of x_D/R for targets of atomic number Z , compared with experiments by Seliger (1955) (○) and Cosslett and Thomas (1964a) (●). $x_D/R = 12/(Z+8)$ is Cosslett's corrected form which is 1.5 times the form predicted by Tomlin (1963).

5. Backscattering

The general form of the variation with thickness in the fraction η_B of the backscattered electrons, which are deflected inside the limiting angle θ_0 subtended by the backscattered radius r_B of the centre of a sphere model, as in figure 1, is assumed to have the same exponential form as η_T , but the absorption factor γ_B must be larger than γ because of diffusion loss due to multiple collisions.

By differentiating (14) with respect to y , using (4) and normalizing by

$$n = \frac{1}{\int_0^{\pi/2} \sin \theta d\theta / (1 + \cos \theta)^{11/6}}$$

we obtain

$$\frac{d\eta_B(y)}{dy} = -\frac{d\eta_T}{dy} D(y) n \int_0^{\theta_0} \frac{\sin \theta d\theta}{(1 + \cos \theta)^{11/6}}$$

where $D(y)$ is the diffusion-loss function of backscattered electrons with respect to y . It may be simply expressed by

$$\begin{aligned} \frac{d\eta_B(y)}{dy} &= \frac{n\gamma}{(1-y)^2} \exp\left(-\frac{n\gamma y}{1-y}\right) \int_0^{\theta_0} \frac{\sin \theta d\theta}{(1 + \cos \theta)^{11/6}} \\ &= \frac{\gamma_B}{(1-y)^2} \exp\left(-\frac{\gamma_B y}{1-y}\right) \int_0^{\theta_0} \frac{\sin \theta d\theta}{(1 + \cos \theta)^{11/6}} \end{aligned} \quad (17)$$

with

$$\gamma_B = 1.9\gamma. \quad (18)$$

Then the backscattering fraction η_B can be obtained by integration:

$$\eta_B = \int_0^y \frac{\gamma_B}{(1-y)^2} \exp\left(-\frac{\gamma_B y}{1-y}\right) dy \int_0^{\theta_0} \frac{\sin \theta d\theta}{(1 + \cos \theta)^{11/6}}.$$

With $\cos \theta_0 = y/(1-y)$, this leads to

$$\eta_B = \frac{6}{5} \int_0^y \frac{\gamma_B}{(1-y)^{7/6}} \exp\left(-\frac{\gamma_B y}{1-y}\right) dy - \frac{6}{5 \times 2^{5/6}} \left\{ 1 - \exp\left(-\frac{\gamma_B y}{1-y}\right) \right\}. \quad (19)$$

The fractional backscattering η_B from several target materials as a function of reduced depth y , as calculated by (19), is shown in figure 6. The present result is rather in closer

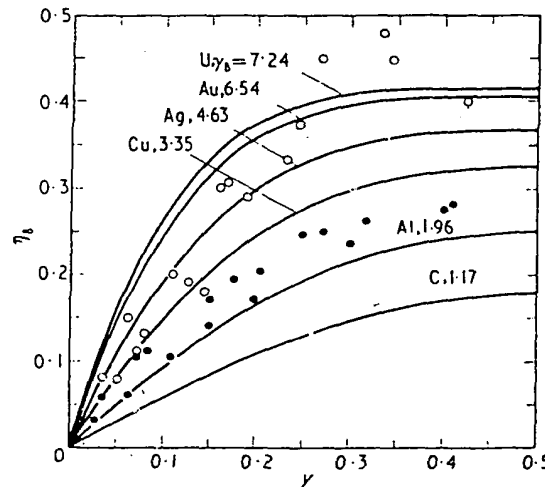


Figure 6. Fractional backscattering η_B from several targets as a function of reduced depth y , compared with experimental results of Cosslett and Thomas (1965) for Cu (●) and Au (○) at 5-20 keV.

agreement with experiment (Cosslett and Thomas 1965) than the existing theories (Archard 1960, Everhart 1960, Archard and Mulvey 1963).

6. Absorption of electrons

Following Cosslett and Thomas, we obtain the fraction η_A of the incident beam absorbed in a solid target by difference:

$$\eta_A = 1 - (\eta_T + \eta_B).$$

If η_T is substituted by (14) and η_B by (19) into the above, η_A becomes

$$\begin{aligned} \eta_A = 1 - \exp\left(-\frac{\gamma y}{1-y}\right) - \frac{6 \times 1.9}{5} \int_0^y \frac{\gamma}{(1-y)^{5/6}} \exp\left(-\frac{1.9\gamma y}{1-y}\right) dy \\ + \frac{6}{5 \times 2^{5/6}} \left\{ 1 - \exp\left(-\frac{1.9\gamma y}{1-y}\right) \right\}. \end{aligned} \quad (20)$$

The absorbed fraction calculated by (20) is in good accord with the results of Cosslett and Thomas (1965), as shown in figure 7.

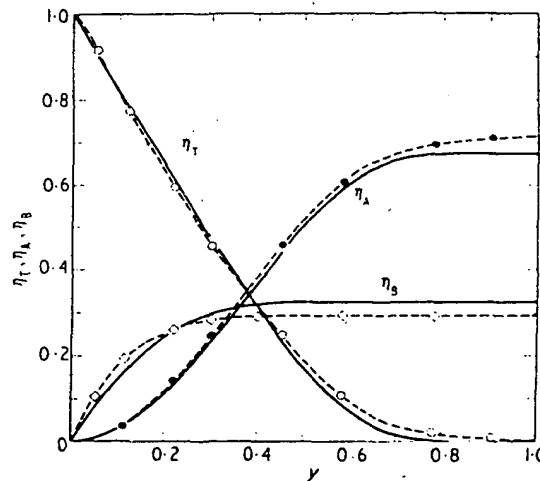


Figure 7. Relative proportions of electrons transmitted (η_T), backscattered (η_B) and absorbed (η_A) in Cu as a function of the reduced depth y . Broken curves and points indicate experimental results of Cosslett and Thomas (1965) for Cu at 10 keV.

The distributions of absorbed electrons at different incident energies can be represented by a single curve for a given element when the normalized fraction is plotted against depth as a fraction of the range y , as suggested by Cosslett and Thomas (1965). The normalized fraction of electrons absorbed per unit mass-thickness is obtained by differentiating (20):

$$\begin{aligned} \rho R \frac{d\eta_A}{d(\rho x)} = \frac{\gamma}{(1-y)^2} \exp\left(-\frac{\gamma y}{1-y}\right) \left\{ 1 + \frac{6 \times 1.9}{5} \exp\left(-\frac{1.9\gamma y}{1-y}\right) \right. \\ \left. \times \left(\frac{1}{2^{5/6}} - (1-y)^{5/6} \right) \right\}. \end{aligned} \quad (21)$$

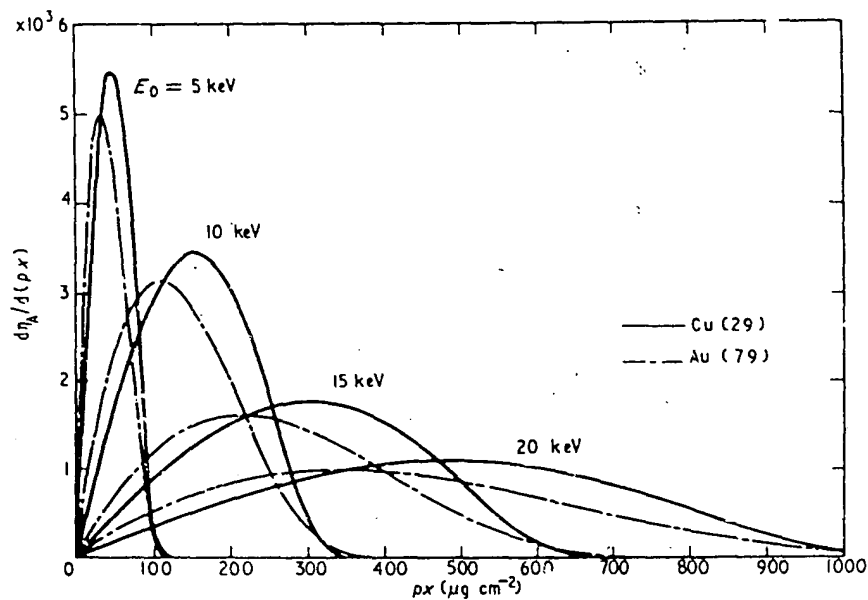


Figure 8. Fraction of electrons absorbed per unit mass-thickness as a function of depth px in solid targets of Cu and Au at 5, 10, 15 and 20 keV. The values at 5 keV are drawn to half scale.

The fraction of electrons absorbed per unit mass-thickness as a function of depth x in solid targets of copper and gold at 5, 10, 15 and 20 keV is shown in figure 8. The distributions for the two elements are very similar at the same incident energy. The variation shows qualitative agreement with the differential absorption evaluated from experimental data of transmitted and backscattered electrons by Cosslett and Thomas.

7. Energy dissipation

The dissipation of energy with depth may be calculated in a similar way to the treatment by Cosslett and Thomas (1965):

$$E_A = E_0 - \eta_T E - \eta_B E_B$$

where E and E_B refer to the energy of transmitted electrons through matter, reduced by electronic collisions as given by (11), and the mean energy of backscattered electrons from a target due to nuclear collisions. Values of E_B/E_0 are provided by several authors (Brand 1936, Kulenkampff and Rüttiger 1954, Kulenkampff and Spyra 1954, Sternglass 1954, Klein 1968), as shown in figure 9. The value that best fitted the curve shown in the figure was used for the present calculation.

We deduce that, corresponding to the above equation, the energy E_A absorbed in the fractional layer of material between the surface and depth x is given by

$$\begin{aligned} \frac{E_A}{E_0} = & 1 - (1-y)^{3/5} \exp\left(-\frac{\gamma y}{1-y}\right) - \frac{E_B}{E_0} \left[\frac{6 \times 1.9}{5} \int_0^y \frac{\gamma}{(1-y)^{7/6}} \right. \\ & \times \exp\left(-\frac{1.9\gamma y}{1-y}\right) dy - \left. \frac{6}{5 \times 2^{5/6}} \left\{ 1 - \exp\left(-\frac{1.9\gamma y}{1-y}\right) \right\} \right]. \end{aligned} \quad (22)$$

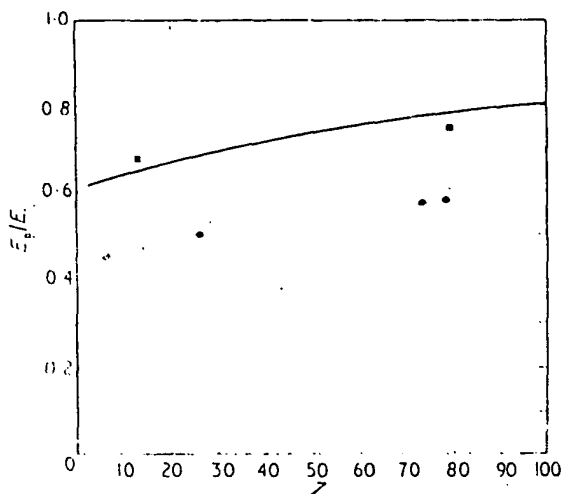


Figure 9. Mean fractional energy of reflected electrons E_B/E_0 against Z , the atomic number. Experimental points: \circ (Brand 1936—32 keV, $\theta=8^\circ$); \bullet (Sternglass 1954—2 keV, $\theta=45^\circ$); \square (Kanter 1957—10 keV, $\theta=15^\circ$); \blacksquare (Kanter 1957—10-70 keV, $\theta=75^\circ$).

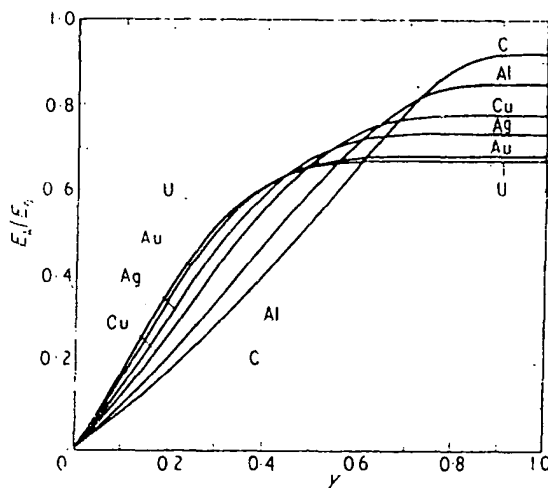


Figure 10. Fraction of energy dissipated E_A/E_0 within a given fraction of the range y in targets of C, Al, Cu, Ag, Au and U.

Figure 10 shows the result calculated by (22) for several target materials. The calculated distributions of the energy explain fairly well the fact that at a given incident energy the curves are first almost coincident, for the energy is retarded due to electronic collisions, but then diverge increasingly owing to the difference in the amount of energy lost by back-scattering due to nuclear collisions. At the end of the range this is equal to the amount $[\eta_B]_{y=1/2} (E_B/E_0)$.

The reduced fraction of energy dissipated in unit mass-thickness $d(E_A/E_0)/d(\rho x)$ can be obtained by differentiating (22):

$$\begin{aligned} \rho R \frac{d(E_A/E_0)}{d(\rho x)} = & \frac{1}{(1-y)^{2/5}} \exp\left(-\frac{\gamma y}{1-y}\right) \left(\frac{\gamma}{1-y} + \frac{3}{8}\right) \\ & + \frac{E_B}{E_0} \frac{6 \times 1.9}{5} \frac{\gamma}{(1-y)^2} \exp\left(-\frac{1.9\gamma y}{1-y}\right) \left(\frac{1}{2^{5/6}} - (1-y)^{5/6}\right). \end{aligned} \quad (23)$$

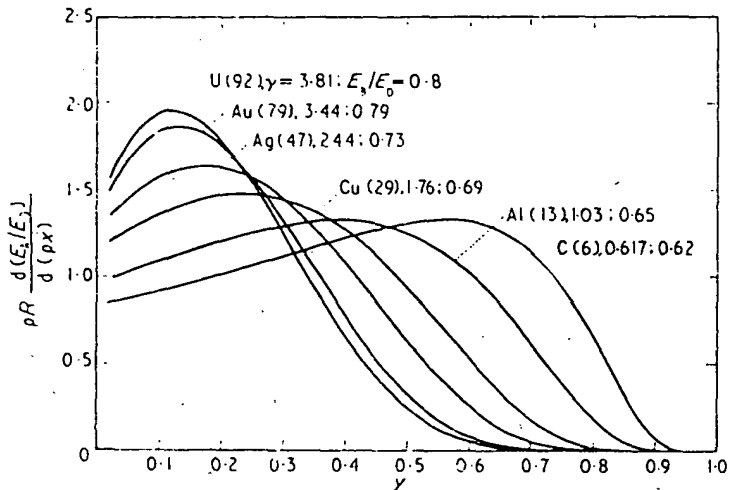


Figure 11. Normalized fraction of energy dissipated in unit mass-thickness as a function of the reduced depth y .

Figure 11 shows the result calculated by (23) for several target materials. In the figure the peak position corresponds to the fraction of maximum energy dissipation depth. Its values are 0.56, 0.38, 0.24, 0.18, 0.14 and 0.12 for carbon, aluminium, copper, silver, gold and uranium. Figure 12 shows the depth-dose function per unit mass-thickness, $dE_A/d(\rho x)$, for two typical target materials of copper and gold, compared with the results by Cosslett and Thomas (1965). The theoretical and experimental distributions show only qualitative agreement, but the peak value is located at almost the same reduced depth. Better agreement would be possible by selecting more appropriate values of ρR and E_B/E_0 .

8. Diffusion model

On the basis of the Bethe energy-loss theory, Archard (1961) proposed the so-called 'diffusion model' of a sphere in which electrons move equally in all directions from the depth of complete diffusion x_D in such a way that their overall paths are equal to the full range R . For a high atomic number this model agrees fairly well with the photograph of electron glow published by Ehrenberg *et al* (1953, 1963); but for a low atomic number it cannot be applied, because backscattered electrons reaching the surface in their original directions vanish. This is because the model disregards electrons undergoing

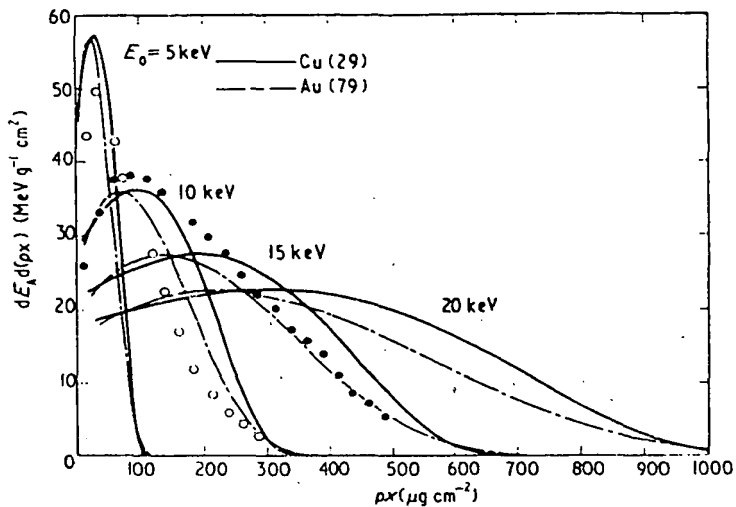


Figure 12. Depth-dose function in solid targets of Cu and Au at 5, 10, 15 and 20 keV, compared with experimental results of Cosslett and Thomas (1965) for Cu (●) at 15 keV and for Au (○) at 10 keV.

large-angle elastic reflection between the surface and the depth of complete diffusion. Accordingly, a modified diffusion model may be assumed which represents the distribution of electrons by a sphere whose centre is located at the depth x_E of energy dissipation; this takes account of both the absorbed electrons and deflected electrons.

The backscattering range r_B is given by

$$r_B = \frac{CR\gamma}{1+\gamma} \quad (24)$$

where the best fitting is obtained by taking $C=1.1$.

The maximum energy dissipation depth x_E can be obtained by a simple geometrical relation:

$$x_E = \frac{R}{2} \left(1 - \frac{C^2 \gamma^2}{(1+\gamma)^2} \right) = \frac{R(1+2\gamma-0.21\gamma^2)}{2(1+\gamma)^2} \quad (25)$$

The values of x_E/R agree with those for the peak in the fractional energy dissipation curves (figure 11). The values of x_E/R are 0.41 (for carbon), 0.34 (aluminium), 0.25 (copper), 0.20 (silver), 0.14 (gold) and 0.12 (uranium), compared with the positions of the energy dissipation peaks: 0.56, 0.38, 0.24, 0.18, 0.14 and 0.12. In elements of low Z , even though the difference is greater than for elements of high Z , we can assume as a first approximation that electrons spread out from points which coincide with the maximum energy dissipation depths.

Then the backscattering coefficient r can be obtained by the following equation:

$$r = \frac{1}{4\pi} \int_0^{\theta_0} 2\pi \sin \theta d\theta = \frac{1}{2} (1 - \cos \theta_0) \quad (26)$$

with

$$\tan \theta_0 = \frac{r_B}{x_E} = \frac{2.2\gamma(1+\gamma)}{1+2\gamma-0.21\gamma^2}$$

The backscattering coefficient r from (26) accords well with the value $\eta_B(y=\frac{1}{2})$ found from (19), as shown in figure 13. The values of r are 0.15 (for carbon), 0.24 (aluminium), 0.33 (copper), 0.38 (silver), 0.42 (gold) and 0.43 (uranium), compared with the back-scattering fractions η_B at the end of the range ($y=\frac{1}{2}$): 0.18, 0.25, 0.33, 0.37, 0.40 and 0.41. Figure 14 represents the modified diffusion models for several target materials, where the broken curves are the original diffusion models.

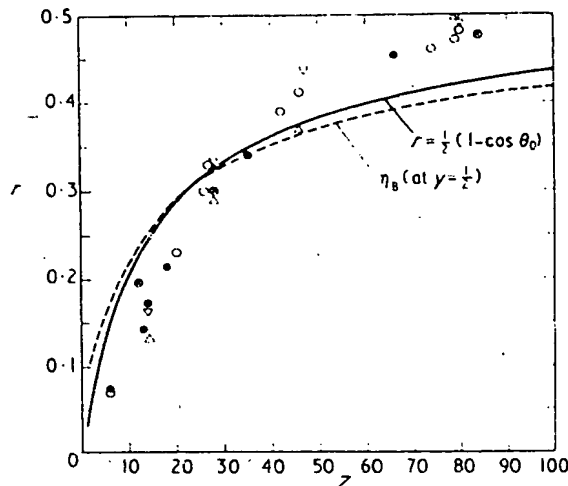


Figure 13. Backscattering coefficient r for atomic number Z according to the modified diffusion model, compared with the results of different authors. Broken curve indicates the backscattering fraction η_B at the end of the range ($y=\frac{1}{2}$). Experimental points were collected by Archard (1961); references will be found therein.

9. Conclusions

The results of interest in connection with the fundamental theory of electron scattering, such as mass-range, transmission, diffusion depth, backscattering, energy loss and maximum energy-loss depth, are consistently expressed in normalized form as a function of the reduced depth y . And, based on the relationship existing between backscattering and energy dissipation, a diffusion model represented by a sphere whose centre is located at the maximum energy dissipation depth is proposed.

The present treatment gives only a first-order approximation to the scattering events of penetrating electrons in a solid target. Better quantitative comparison between theoretical and experimental results may be obtained by using corrected values of the parameters λ_s , γ and γ_B which have been arbitrarily assumed on an empirical basis because they are independent of the fundamental course of the theory. However, in the case of high voltages above 1 MeV, the power-potential law with $s=\frac{1}{2}$ cannot be applied. It seems that the Rutherford scattering theory and Bethe energy-loss law are more realistic expressions in such a case. According to the same treatment, by using the Rutherford scattering model with $s=1$, the absorption parameter γ is given by

$$\gamma = \frac{cZ}{\ln(E_0/13.5Z)}$$

where

$$c = 0.1 \sim 0.3.$$

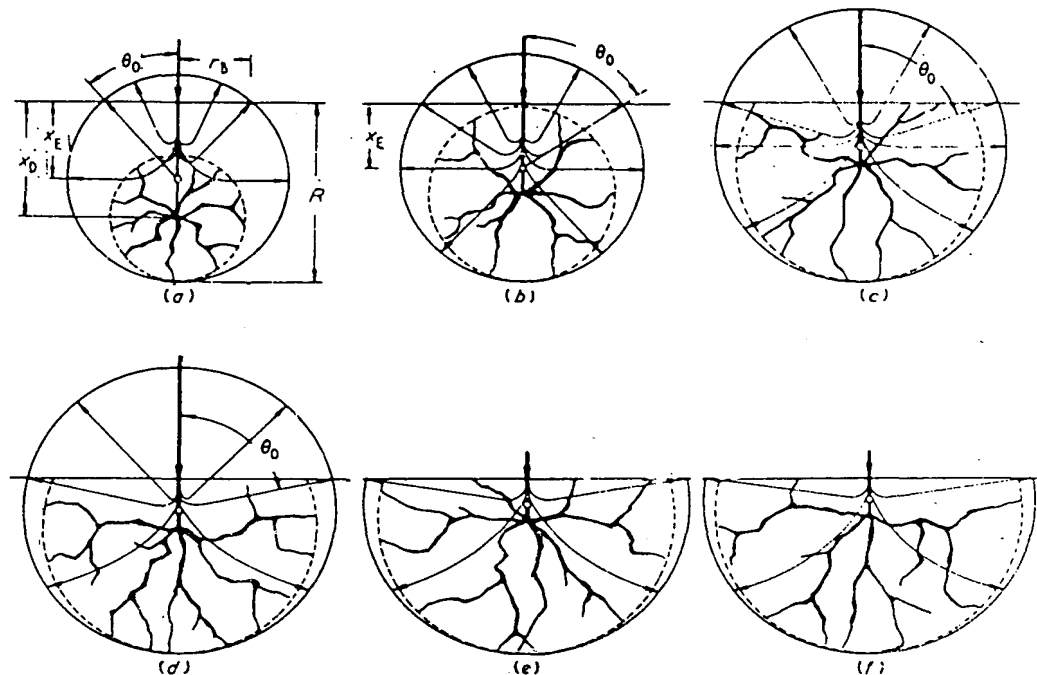


Figure 14. Representation of modified diffusion models for several targets:

Target	γ	x_D/R	x_E/R	r	r_n/R
(a) C (6)	0.617	0.618	0.412	0.150	0.420
(b) Al (13)	1.03	0.491	0.344	0.238	0.559
(c) Cu (29)	1.76	0.362	0.253	0.330	0.792
(d) Ag (47)	2.44	0.291	0.196	0.378	0.780
(e) Au (79)	3.44	0.225	0.137	0.421	0.852
(f) U (92)	3.81	0.208	0.120	0.432	0.871

The distributions of η_T , η_B , η_A and E_A vary slightly with the accelerating voltage. If more reliable data for comparison become available, the continued treatment by the Rutherford scattering model will be reported elsewhere.

Acknowledgments

The authors wish to thank Dr V E Cosslett, Cavendish Laboratory, University of Cambridge, for helpful comments and valuable advice in connection with the publication of this paper, and Dr H Kawakatsu for frequent and helpful discussions.

References

Archard GD 1961 *J. appl. Phys.* **32** 1505-9
 Archard GD and Mulvey T 1963 *Br. J. appl. Phys.* **14** 626-34
 Berger MJ and Seltzer SM 1964 *Tables of Energy Losses and Ranges of Electrons and Positrons*, NASA, SP-3012
 Bethe HA 1933 *Handb. Phys.* **24** 519 (Berlin: Springer-Verlag)

Bethe H A, Rose M E and Smith L P 1938 *Proc. Am. Phil. Soc.* **78** 583-5
 Bishop H E 1965 *Proc. Phys. Soc.* **85** 855-66
 —— 1967 *Br. J. appl. Phys.* **18** 703-15
 Bothe W 1933 *Handb. Phys.* **22/2** 1 (Berlin: Springer-Verlag)
 —— 1949 *Ann. Phys., Lpz.* **6** 44-52
 Brand J O 1936 *Ann. Phys., Lpz.* **26** 609-24
 Cosslett V E 1964 *Br. J. appl. Phys.* **15** 107-9
 Cosslett V E and Thomas R N 1964a *Br. J. appl. Phys.* **15** 883-907
 —— 1964b *Br. J. appl. Phys.* **15** 1283-300
 —— 1965 *Br. J. appl. Phys.* **16** 779-96
 Dashen R F 1964 *Phys. Rev.* **134** A1026-32
 Ehrenberg W and Franks J 1953 *Proc. Phys. Soc. B* **66** 1057-66
 Ehrenberg W and King D E N 1963 *Proc. Phys. Soc. B* **81** 751-66
 Everhart T E 1960 *J. appl. Phys.* **31** 1483-90
 Goudsnit S and Saunderson J L 1940 *Phys. Rev.* **57** 24-9
 Kanaya K, Shimizu K and Ishikawa Y 1968 *Br. J. appl. Phys.* **2** 1657-65
 Kanter H 1957 *Ann. Phys., Lpz.* **20** 144-66
 Klein C A 1968 *Tech. Memo., Raytheon Co T-786* pp 1-8
 Kulenkampff H and Rüttiger K 1954 *Z. Phys.* **137** 426-34
 Kulenkampff H and Spyra W 1954 *Z. Phys.* **137** 416-25
 Lenard P 1895 *Ann. Phys., Lpz.* **56** 255
 —— 1918 *Quantitatives über Kathodenstrahlen aller Geschwindigkeiten* (Heidelberg: Karl Winters Universitäts Buchh.).
 Lenz F 1954 *Z. Naturf.* **99** 185-204
 —— 1958 *Z. angew. Phys.* **10** 31-4
 Lindhard J, Scharff M and Schiott H E 1963 *K. danske Vidensk. Selsk., Math.-phys. Meddr.* **33** 1-42
 Makhov A E 1960a *Sov. Phys.-Solid St.* **2** 1934-41
 —— 1960b *Sov. Phys.-Solid St.* **2** 1942-4
 —— 1960c *Sov. Phys.-Solid St.* **2** 1945-51
 Marton L, Simpson J A, Fowler H A and Swanson N 1962 *Phys. Rev.* **126** 182-92
 Meister H 1958 *Z. Naturf.* **13a** 809-20
 Molière H 1947 *Z. Naturf.* **2a** 133-45
 —— 1948 *Z. Naturf.* **3a** 78
 Reimer L 1968 *Optik* **27** 86-98
 Schumacher B W 1967 *Westinghouse Res. Rep. Sci. Paper 67-1c2-EWEID-PI* pp 1-16
 Seliger H H 1955 *Phys. Rev.* **100** 1029-37
 Shimizu R and Shinoda G 1963 *X-ray Optics and X-ray Microanalysis* ed H H Pattee, V E Cosslett and A Engström (New York: Academic Press) pp 419-30
 Smith G H and Burge R E 1963 *Proc. Phys. Soc.* **81** 612-32
 Spencer L V 1955 *Phys. Rev.* **98** 1597-615
 Sternglass E J 1954 *Phys. Rev.* **95** 345-58
 Tomlin S G 1963 *Proc. Phys. Soc.* **82** 465-66
 Wentzel G 1922 *Ann. Phys., Lpz.* **69** 335-68
 —— 1927 *Z. Phys.* **40** 590-3